Transactions of Materials Research 1 (2025) 100040

Contents lists available at ScienceDirect

Transactions of Materials Research

journal homepage: www.sciencedirect.com/journal/transactions-of-materials-research

# Neon-induced suppression of deuterium retention in tungsten: Effects of temperature and Ne concentration

Ying Qin [a], Long Cheng [a], Yue Yuan [a,*], Yuhao Li [a], Di Hu [a], Sijie Hao [a], Arkadi Kreter [b], Guang-Hong Lu [a]

[a] School of Physics, Beihang University, Beijing, 100191, People's Republic of China
[b] Forschungszentrum Jülich GmbH, Institute of Fusion Energy and Nuclear Waste Management - Plasma Physics, Jülich, 52425, Germany

ARTICLE INFO

*Keywords:*
Tungsten
Neon seeding
Deuterium retention
Blistering
Sputtering

ABSTRACT

Neon (Ne) seeding is a key strategy for radiative cooling in the divertor to mitigate extreme thermal loads and protect plasma-facing materials in future fusion devices. This study investigates the effects of Ne seeding on tungsten (W) surface morphology and deuterium (D) retention under plasma irradiation conditions relevant to fusion reactors. Experiments were conducted using W samples exposed to pure D, sequential D-Ne (Ne pre-irradiation followed by D exposure), and mixed D-Ne plasmas with different Ne concentrations, at temperatures of 500 K and 1200 K with ion fluxes of $1.0 \times 10^{22}$ $m^{-2}s^{-1}$ and $1.2 \times 10^{24}$ $m^{-2}s^{-1}$, respectively, in the linear plasma facilities PSI-2 and Pilot-PSI. At low temperature (500 K), sequential D-Ne irradiation significantly increases surface roughness and completely suppresses D-induced blister formation. In contrast, mixed D-Ne irradiation under identical conditions leads to micron-sized blisters with fractured caps. At high temperatures (~1200 K), mixed D-Ne irradiation entirely prevents blister formation, whether the Ne concentration is 5 % or 20 %. In addition, under the exposure conditions employed in this study, Ne seeding consistently resulted in a reduction in D retention. At 500 K, D retention decreased by up to 50 %, whereas at 1200 K, it was reduced by approximately 30 % for 5 % Ne concentration and dropped below the detection limit for 20 % Ne concentration. The suppression of deuterium retention in tungsten due to neon seeding is attributed to sputtering-induced surface erosion and the Ne-vacancy complexes that pin the trapped D atoms, thereby inhibiting blister formation. These findings underscore the potential of Ne as an effective radiative cooling impurity in fusion devices and provide valuable insights into optimizing the performance of plasma-facing materials.

## 1. Introduction

The divertor as a critical component is subjected to extreme thermal loads in future fusion reactors. To mitigate the heat flux on the divertor surface and protect plasma-facing materials (PFMs), the injection of radiative cooling impurities has become an essential strategy for high-power operations, as demonstrated in ITER, DEMO [1,2]. Seeding impurities such as nitrogen (N), neon (Ne), or argon (Ar) into the divertor enhances radiative cooling, effectively reducing thermal loads and extending the divertor's operational lifetime [3–5].

Tungsten (W) is the preferred material for the divertor in tokamak devices, owing to its high melting point, superior thermal conductivity, low sputtering yield, minimal hydrogen isotope retention et al. [6]. However, impurity seeding profoundly affects the W-plasma interaction, influencing surface morphology modification and hydrogen isotope retention [7–9].

Among the seeding impurities, Ni chemically interacts with W, resulting in a mixed surface layer, exacerbating deuterium (D) retention and surface blistering [10,11]. In contrast, Ne and Ar, as inert gases, do not react with W but have been confirmed to influence D atom transport and retention primarily through mechanisms such as sputtering and precipitation [9,12]. In particular, Ne, with its low atomic number, is considered to have potential advantages in reducing D retention and mitigating surface damage, similar to the role of helium (He) [13]. Consequently, Ne is among the most extensively utilized radiative cooling impurities in fusion devices.

Previous studies have demonstrated that the impact of Ne on D behavior, including blistering and retention in W, is regulated by several factors, such as temperature, incident particle energy, and ion fluence [9,12,14,15]. Under low temperature and high incident particle energy

* Corresponding author.
*E-mail address:* yueyuan@buaa.edu.cn (Y. Yuan).

https://doi.org/10.1016/j.tramat.2025.100040
Received 7 April 2025; Received in revised form 13 April 2025; Accepted 12 May 2025
Available online 15 May 2025

conditions (500 K, 70 eV), Ne seeding increases D retention by generating small-scale lattice defects through atomic displacement traps for D atoms in the near-surface layer. In contrast, under relatively high-temperature conditions (700 K, 70 eV), the precipitation effect of Ne may predominate in D transport, leading to reduced D retention [9,16]. Under conditions of low temperature and low incident energy (550 K, 40 eV), Ne seeding modifies the sub-surface structure, promoting D atom recombination on the W surface and providing additional channels for D diffusion out of the W material, thereby reducing D retention [13]. These findings further underscore the imperative for thoroughly investigating the impact mechanisms of Ne seeding into the D plasma under different plasma settings, particularly regarding D trapping and retention mechanisms, to elucidate the impact of factors such as temperature, dose, and impurities on the performance of tungsten materials and the preservation of hydrogen isotopes in W, which is essential for maintaining tritium fuel in fusion reactors. Furthermore, although the surface temperature of PFMs during deuterium-tritium (D-T) plasma operation spans a wide range (373–1423 K) [17], systematic studies on Ne seeding at high temperatures remain limited.

This study investigates the effects of Ne seeding on W surface morphology and deuterium retention under diverse plasma irradiation conditions. By conducting sequential and mixed D-Ne plasma irradiation experiments on W samples in the linear plasma facilities PSI-2 and Pilot-PSI, we aim to understand how Ne suppresses D retention and blistering across a range of temperatures and Ne concentrations.

## 2. Experiment

### 2.1. Original material

The W samples used in this study were cut from a W sheet with a purity of 99.95 wt% and a rolling reduction of 80 %, supplied by Advanced Technology & Materials Co., Ltd. The W grains with an average grain size of 2–5 μm exhibited an elongated distribution along the irradiation surface. The characterization of the W sample is detailed in Ref. [18]. To accommodate different linear plasma devices, the samples were cut into two shapes: a thin rectangular plate with dimensions of $10 \times 10 \times 1.5$ mm$^3$ and a top-hat shape with a front surface of $10 \times 15$ mm$^2$ and an under-surface of $15 \times 15$ mm$^2$. Before irradiation, all samples were mechanically polished using silicon carbide sandpaper, followed by electrochemical polishing in a 1 wt% sodium hydroxide solution to achieve a mirror-like surface finish. Subsequently, under high vacuum conditions ($<1 \times 10^{-3}$ Pa), the thin rectangular plate samples were annealed at 1973 K for 1 h to ensure complete recrystallization, referred to as recrystallized W. The top-hat shape samples were annealed at 1273 K for 1 h to remove surface residual stress, referred to as rolled W. Further characterization details regarding the two W samples can be found in Refs. [19,20].

### 2.2. Plasma exposures

This study was designed to conduct two series of plasma exposure experiments, with low-temperature exposures conducted in the linear plasma generator PSI-2 at Forschungszentrum Jülich, Germany [21,22], and high-temperature exposures performed with the linear plasma device Pilot-PSI at the DIFFER [23].

For the experiments on PSI-2, recrystallized W samples with the shape of a thin rectangular plate were exposed to pure D plasma, sequential D-Ne plasma (Ne plasma pre-irradiation), and mixed D-Ne plasma. In the Ne seeding exposure, the flow ratio of Ne to D was set at 1:10 for the sequential D-Ne plasma exposure, and a concentration of Ne ions was 10 % for the mixed D-Ne plasma exposure. The D fluence with a constant data of $1.0 \times 10^{26}$ D/m$^2$. The Ne content was monitored in real time by optical emission spectroscopy. The exposure temperature was 500 K, and the D and Ne incident ion energy was ~40 eV, close to the sputtering threshold of Ne in W [24], controlled by a negative bias potential [9]. Plasma parameters were measured using a Langmuir probe, with an electron density of $\sim 10^{18}$ m$^{-3}$, an electron temperature of ~10 eV, and an incident ion flux of $1.0 \times 10^{22}$ D m$^{-2}$s$^{-1}$.

The rolled W samples were exposed to pure D and mixed D-Ne plasmas for the higher temperature (~1200 K) and higher flux plasma exposure experiments conducted on Pilot-PSI, which employs a cascaded arc plasma source, generating an ultra-high-density plasma of approximately $10^{24}$ D m$^{-2}$s$^{-1}$ [25]. In this experimental series, the Ne ion concentrations in the mixed D-Ne plasma were set at 5 % and 20 % [13], referred to as D-5Ne and D-20Ne in the subsequent text. The D fluence was fixed at $\sim 3.0 \times 10^{26}$ D m$^{-1}$. The incident energy of ~40 eV for both D and Ne ions. The plasma electron density exhibits a Gaussian radial distribution with a peak value of $\sim 2.0 \times 10^{20}$ m$^{-3}$ and a full width at half maximum of ~11 mm. The electron temperature remains relatively uniform at ~1.1 eV. According to the Bohm criterion, the flux of D plasma is $\sim 1.2 \times 10^{24}$ D m$^{-2}$s$^{-1}$. The total exposure duration is ~300s. Due to the rapid heating process, the influence of the heating phase on the results is not emphasized in this paper. The surface temperature distribution was measured using an infrared camera (FLIR SC7500-MB) with an emissivity setting of 0.05, and the measurement uncertainty was ~10 K. Due to the samples with temperatures exceeding 850 K, a multi-wavelength pyrometer (FAR FMPI) was used to monitor the surface temperature in real-time. The advantage of the pyrometer is that its temperature output is independent of the emissivity of the surface of the materials. During irradiation, the temperatures measured at the center and edge of the samples by the infrared camera were corrected based on the pyrometer readings. More details of the experiment can be found in Refs. [13,26].

The names of all samples used in this experiment, along with their corresponding experimental conditions and deuterium retention results, are summarized in Table 1.

### 2.3. Characterization

After plasma exposure, the modification of the W sample surface morphology was observed using scanning electron microscopy (SEM). Cross-sections of blisters on the W samples were prepared and analyzed using a focused ion beam (FIB). The orientation distribution of W grains after Ne plasma pre-irradiation was examined using electron backscattering diffraction (EBSD).

The depth distribution of D in W samples exposed to the PSI-2 device was determined using nuclear reaction analysis (NRA) based on the D ($^3$He, p)$^4$He reaction, where a $^3$He ion beam with a spot diameter of 1 mm was used to irradiate the central region of the sample. The energy of the $^3$He ion beam was 4.4 MeV, with a detection depth of approximately 7 μm. By detecting the energy spectra of protons and alpha particles ($^4$He) produced in the reaction, the spectra were analyzed using the SIMNRA software to obtain the depth distribution of D retention. The relative accuracy of both NRA and TDS methods typically ranges from 10 % to 20 %, with greater uncertainty for samples with less retained deuterium.

For samples tested on Pilot-PSI, Positron Annihilation Doppler Broadening Spectroscopy (PADB) was employed to characterize vacancy-type defects within a depth of 350 nm. Positrons were generated from a $^{22}$Na source, moderated to thermal energy, and then accelerated by an electric field before being directed onto the sample surface. The positron energy was adjustable in the range of 0.1–25 keV, with a beam intensity of approximately $10^4$ positrons/s and a beam spot diameter of about 8 mm. The positron implantation depth $z$ in the material is related to the incident positron energy [27], with 25 keV positrons having a range of approximately 400 nm in W. Note that, to accurately analyze the impact of plasma irradiation on the near-surface vacancy-type defect characteristics of rolled W, an unirradiated W sample, referred to as blank W, was included as a reference.

The depth profile of D concentration near the W surface was determined by Elastic Recoil Detection Analysis (ERDA), which measures D

**Table 1**
Overview of key plasma conditions and deuterium retention for all exposed samples.

| sample | device | $T_s$ (K) | $E_i$ (eV) | Ne ion fluence ($m^{-2}$) | D ion fluence ($m^{-2}$) | D retention NRA ($D/m^2$) (depth <7 μm) | D retention TDS ($D/m^2$) |
|---|---|---|---|---|---|---|---|
| Pure D-LT | PSI-2 | 500 | 40 | / | $1.0 \times 10^{26}$ | $1.48 \times 10^{20}$ | $1.94 \times 10^{20}$ |
| Sequential D-Ne | PSI-2 | 500 | 40 | $1.0 \times 10^{25}$ | $1.0 \times 10^{26}$ | $6.10 \times 10^{19}$ | $9.70 \times 10^{19}$ |
| Mixed D-10Ne | PSI-2 | 500 | 40 | $1.1 \times 10^{25}$ | $1.0 \times 10^{26}$ | $6.90 \times 10^{19}$ | $1.06 \times 10^{20}$ |
| Pure D-HT | Pilot-PSI | 1173 | 40 | / | $3.0 \times 10^{26}$ | / | $1.14 \times 10^{19}$ |
| Mixed D-5Ne-HT | Pilot-PSI | 1273 | 40 | $1.5 \times 10^{25}$ | $3.0 \times 10^{26}$ | / | $8.02 \times 10^{18}$ |
| Mixed D-20Ne-HT | Pilot-PSI | 1193 | 40 | $7.5 \times 10^{25}$ | $3.0 \times 10^{26}$ | / | Below detection limit |

concentration distributions up to a depth of 350 nm. During ERDA measurements, heavier elements are used to bombard lighter atoms, and the recoiled lighter atoms are detected to obtain their depth-dependent concentration profiles in the material.

The total D retention was measured using thermal desorption spectroscopy (TDS). The test samples were placed in a vacuum chamber and heated from room temperature to >1273 K at a heating rate of 1 K/s. During the heating process, the signals of $D_2$ (mass 4) and HD (mass 3) were recorded using a sensitive quadrupole mass spectrometer. The total D retention was calculated based on the contributions of $D_2$ and HD, with other D-containing gas molecules having negligible signals. The uncertainty of the TDS measurement was approximately 5 %.

## 3. Results

### 3.1. Surface modification

For the sequential D-Ne samples, the surface morphology after Ne plasma pre-irradiation is observed, as shown in Fig. 1. Ne plasma exposure can cause pronounced surface erosion due to sputtering effects of Ne seeding, significantly increasing the surface roughness of W (Fig. 1 (a) and (c)). Additionally, the degree of sputtering loss varies significantly between different grains. EBSD results in Fig. 1(b) and (d) further show that the sputtering yield of Ne on the W surface depends strictly on grain orientation. Grains with a {111} orientation exhibit the lowest sputtering, indicating the highest resistance to sputtering, while {110} grains show moderate sputtering, and {001} grains display the highest sputtering yield. These results emphasize the sputtering effect of Ne on the W surface, demonstrating a pronounced dependence on grain orientation.

Fig. 2 compares the surface morphology and blister cross-sectional features of W samples after pure D and mixed D-10Ne plasma exposure at 500 K. As shown in Fig. 2(a1), the surface subjected to pure D plasma exposure exhibits micron-sized blisters with intact caps. In contrast, under mixed D-10Ne plasma exposure (Fig. 2(b1)), the blister caps display extensive rupture and heavy erosion at the boundary, consistent with observations reported by Kreter et al. [9]. Additionally, wavy nanostructures, resulting from Ne impurity-induced sputtering,

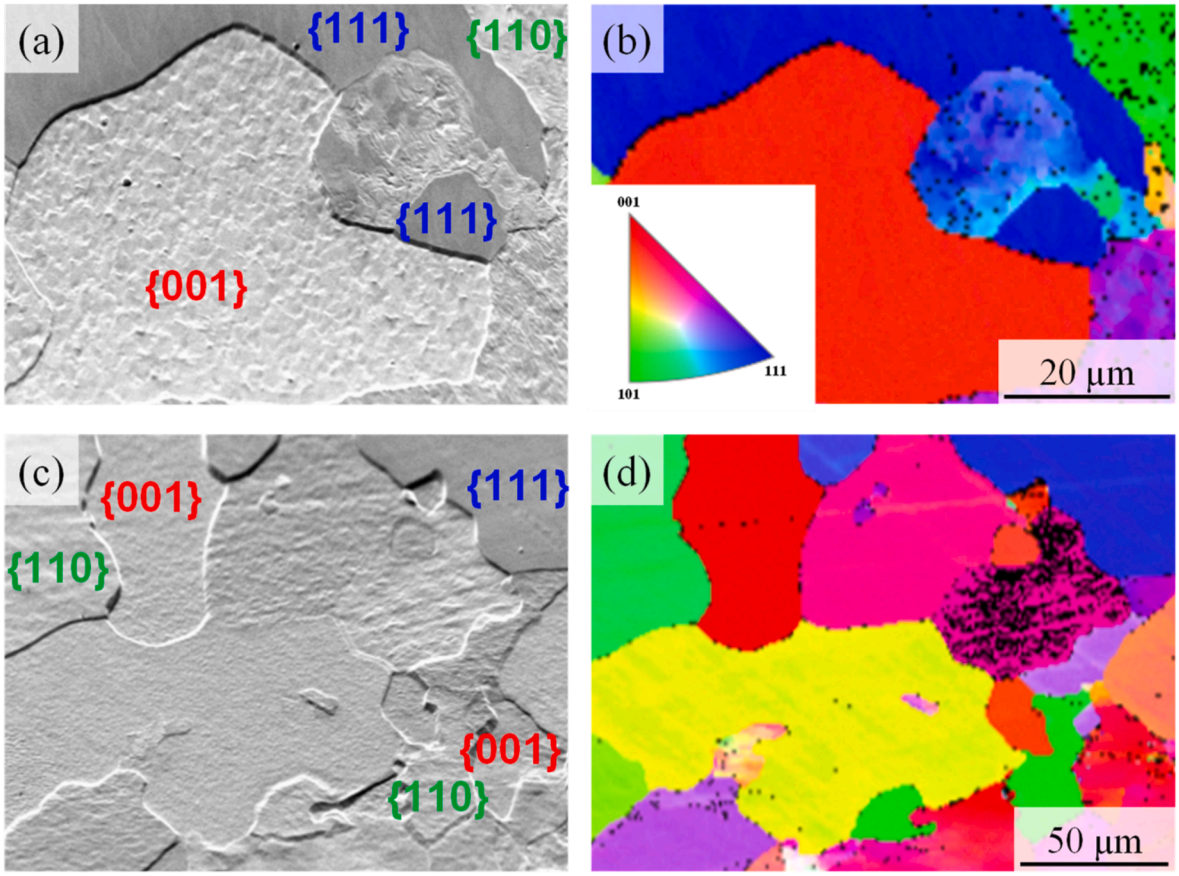


**Fig. 1.** Surface morphology of W sample after Ne plasma irradiation (a) and (c), with the corresponding IPF maps of the surface normal direction (b) and (d). The crystal orientations {001}, {110}, and {111} are indicated at the corresponding grains in the SEM images.

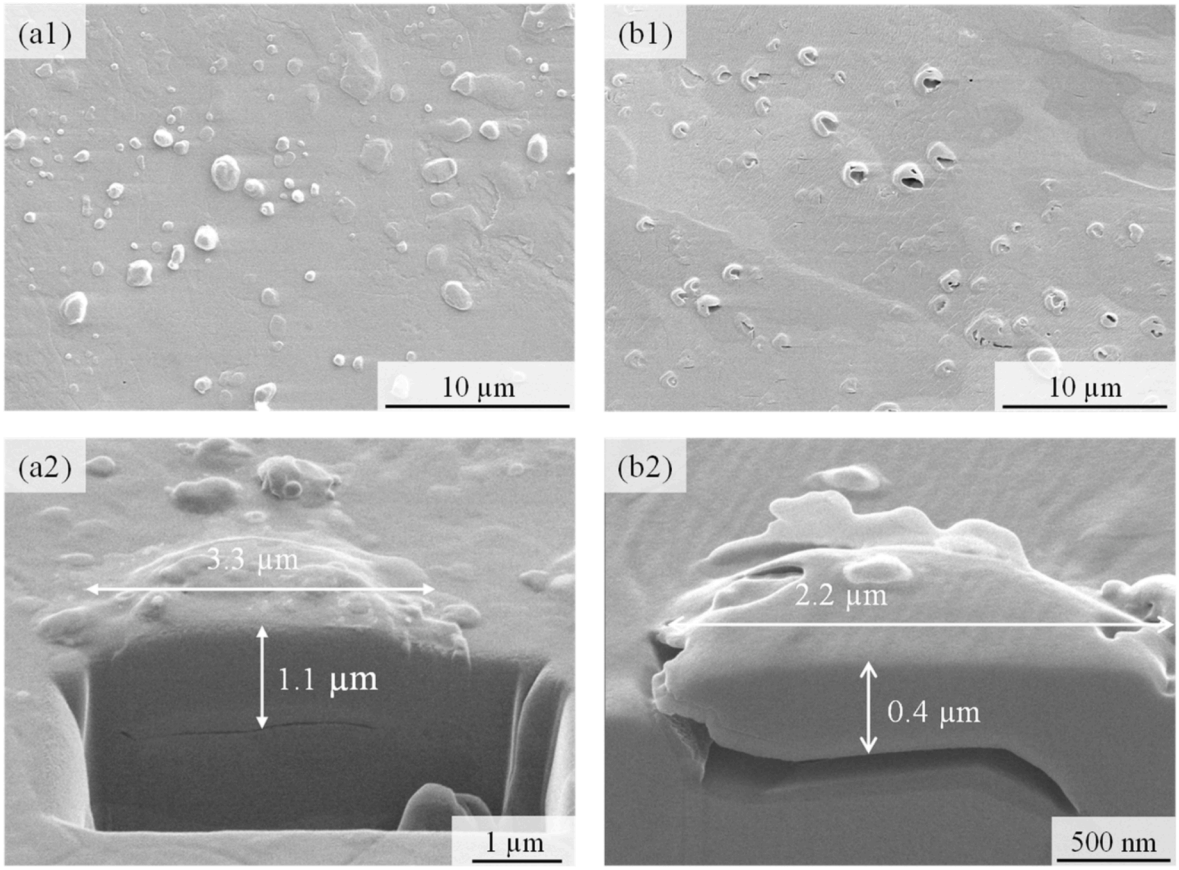


**Fig. 2.** Surface morphology and FIB cross-sectional view of blister after plasma exposure at 500 K. (a1 and a2) pure D-LT, (b1 and b2) mixed D-10Ne plasma. Notably, cross sections are taken from the blister of the {111} grain surface.

are uniformly distributed across the sample surface and the blister caps, accompanied by localized fine cracks. The synergistic effect of D and Ne irradiation reduces the rupture resistance of the blister caps and weakens the structural integrity of the blister caps.

To further analyze the effect of Ne seeding on the sub-surface structure of blisters, cross-sections of grains with {111} orientation from both samples were prepared using FIB and observed, as shown in Fig. 2(a2) and (b2). The seeding of Ne reduces the blister size (from 3.3 μm to 2.2 μm) and thins the blister caps (from 1.1 μm to 0.4 μm), as Ne sputtering away a portion of the blister cap thickness, rendering larger blisters visually smaller and smaller ones invisible under the mixed D-10Ne plasma condition [15].

To investigate the effect of the Ne pre-irradiation on the D behavior, surface morphology changes at the same position are analyzed. Fig. 3 illustrates the surface modification of the sequential D-Ne sample before and after Ne irradiation at the identical position. Fig. 3(a) shows the detailed features of the erosion after Ne pre-irradiation, the W surface develops distinct wavy nanostructures, attributed to the sputtering effect of Ne impurity ions [28–30]. Following successive D plasma exposure, the surface roughness of the sample increases, and the wavy nanostructures in the sputtered area become more apparent (Fig. 3(b)). Notably, no surface blistering is observed. This indicates that the D plasma primarily enhanced surface erosion rather than promoting blistering. This contrasts with the behavior observed under mixed D-10Ne plasma exposure, where blister formation occurs despite the presence of Ne (Fig. 2(b1)). In summary, Ne pre-irradiation effectively suppresses

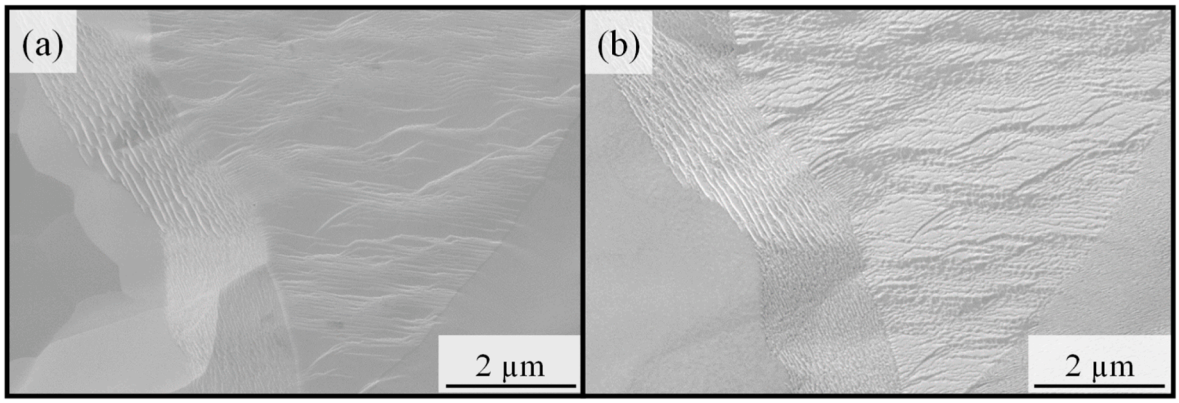


**Fig. 3.** The surface morphology of the sequential D-Ne sample after Ne pre-irradiation (a) and the same position after exposed to subsequent D irradiation (b).

D-induced blistering during sequential Ne-D plasma exposure. However, this effect is not observed when Ne is seeded into D plasma, leading to the formation of blisters instead.

The surface morphology of W after high-temperature (~1200 K) exposure to pure D and D-Ne mixed plasmas in the Pilot-PSI device is shown in Fig. 4. Compared to the pristine W surface, the pure D-HT sample exhibits no significant macroscopic modifications. However, a more detailed examination reveals that D plasma induces a certain degree of surface etching (Fig. 4(a1)). The etching patterns vary across grain surfaces, and significant erosion is observed at the grain boundaries. At higher magnification, high-density triangular pores, approximately 100 nm in size, are observed on certain grain surfaces (Fig. 4 (a2)), likely resulting from the rupture of D-induced blisters [30]. Additionally, a small number of micro-blister structures (~100 nm in size) with low number density are observed on some flat grains (Fig. 4 (a3)).

In contrast to pure D irradiation, the seeding of Ne significantly alters the surface modification of W under D plasma exposure. Under D-5Ne conditions, no blister formation is observed on the sample surface (Fig. 4 (b1)). However, significant erosion is evident at the grain boundaries (Fig. 4(b2)), though to a lesser extent compared to pure D-HT irradiation. Furthermore, small pores (Fig. 4(b2)) and granular structures (Fig. 4(b3)) are distributed across specific grain surfaces, indicating localized surface modifications induced by the combined effects of D and Ne irradiation. When the Ne concentration is increased to 20 %, the sputtering effect of Ne is further enhanced. The surface of the mixed D-20Ne-HT sample develops severe wavy nanostructures (Fig. 4(c1)-(c3)), accompanied by a significant increase in surface roughness. The density of these wavy structures ranges from 5 to 28 $\mu m^{-1}$. Notably, no D-induced blistering formation is observed at either 5 % or 20 % Ne concentrations, indicating that Ne seeding effectively suppresses blister formation at high temperatures, contrasting with the small blisters observed under pure D irradiation.

### 3.2. Deuterium behaviors

Fig. 5 presents the TDS results for the W samples exposed to pure D and D-Ne plasmas at 500 K. A primary desorption peak is observed at ~700 K for both pure D and mixed D-Ne samples. The peak positions of the two samples are similar, but the peak intensity of mixed D-10Ne-LT is weaker, indicating that the same type of defect is responsible for the 700 K desorption peak; however, this defect is less prevalent in mixed D-10Ne-LT. In contrast, the primary desorption peak for sequential D-Ne exposure appears at ~770 K, suggesting that D is trapped in defects with a higher binding energy. Apart from the 770 K peak, an extra desorption peak appears at ~830 K.

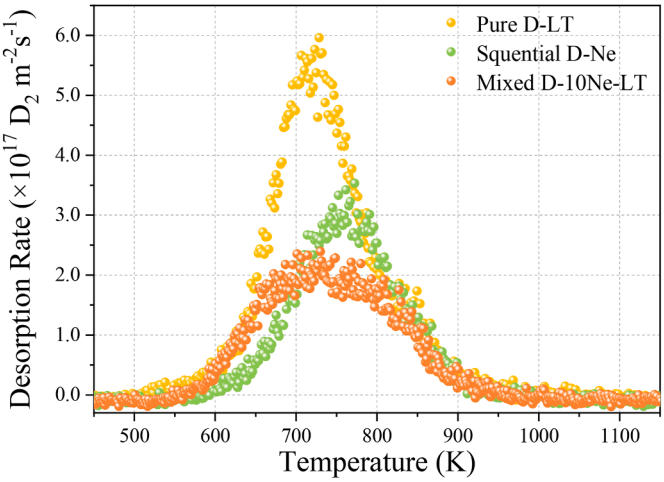


**Fig. 5.** Thermal desorption spectra of the W samples after pure D and D-Ne plasma exposure at low temperature (500 K) conducted on PSI-2.

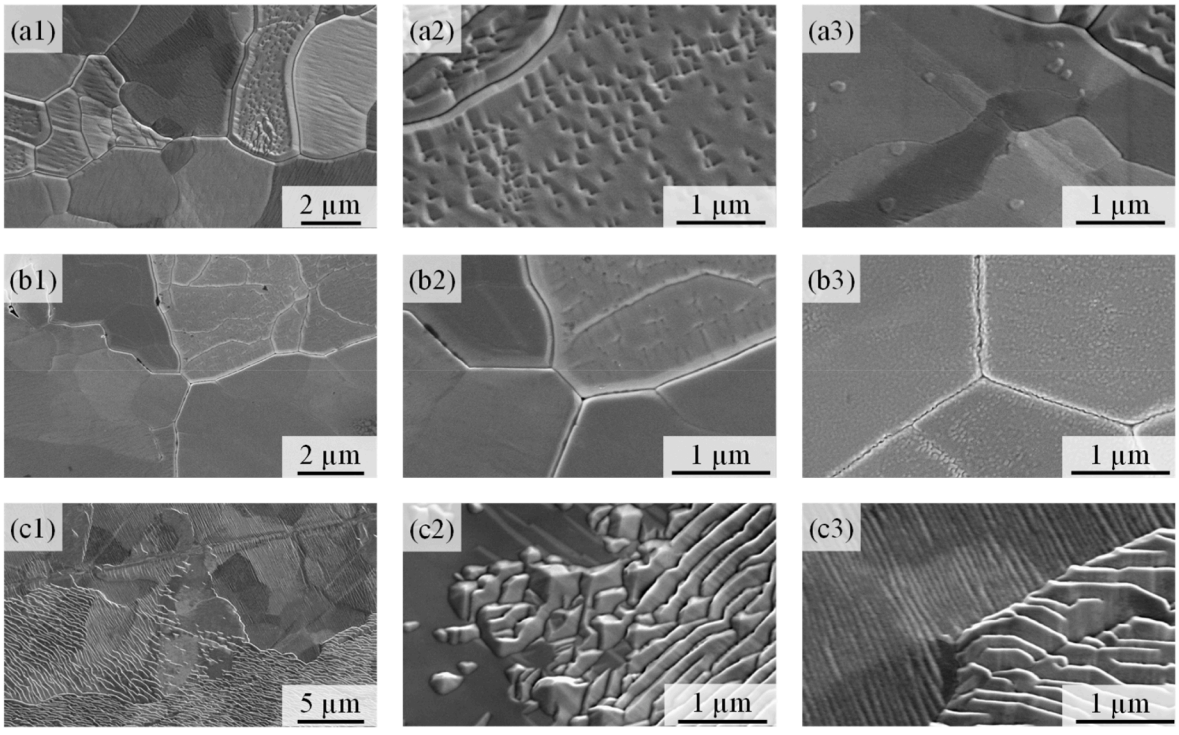


**Fig. 4.** Surface morphology of rolled W after high temperature (~1200 K) plasma exposures conducted on Pilot-PSI. (a) pure D-HT, (b) Mixed D-5Ne-HT, (c) Mixed D-20Ne-HT.

In addition, NRA measurements were performed to determine the D retention in the near-surface region (<7 μm) of the three samples, while TDS was used to calculate their total D retention in the whole bulk. The D retention results are summarized in Table 1. The total D retention is reduced by half under either sequential Ne-D plasma or mixed D-10Ne plasma exposure, demonstrating that Ne seeding effectively suppresses D retention in W. Furthermore, compared with the total D retention from TDS, the NRA data is lower than the total D retention, suggesting that the diffusion depth of D exceeds 7 μm under all three irradiation conditions. The comparative analysis of TDS and NRA data will be discussed in Section 4.2.

Fig. 6(a) illustrates the depth distribution of D concentration within the top 350 nm of the W surface, measured by ERDA. Both pure D-HT and mixed D-5Ne-HT samples have a similar distribution of the D concentration, which increases with depth, reaching a maximum of ~0.3–0.4 at. % at 350 nm in depth. The region beyond 350 nm likely still contains D, due to D diffusing into the deeper bulk at higher temperatures. However, the D signal is not detected in the mixed D-20Ne-HT sample, as its concentration fell below the ERDA detection limit (~$10^{17}$ D $m^{-2}$).

Fig. 6(b) presents the TDS results for $D_2$ in the irradiated W samples at ~1200 K. Both pure D-HT and mixed D-5Ne-HT samples exhibit a single desorption around 1100 K, with the peak for D-5Ne-HT slightly lower than that for pure D-HT. In contrast, the D desorption peak is not observed in the mixed D-20Ne-HT sample, resulting from its D retention being below the TDS detection limit (~$10^{17}$ D $m^{-2}$). Additionally, the total D retention for all three samples is listed in Table 1. The results suggest that Ne seeding significantly reduces D retention at high temperatures and high plasma flux. The mixed D-5Ne-HT sample exhibits a ~30 % decrease in D retention compared to the pure D-HT sample, while the mixed D-20Ne-HT sample shows an even more pronounced reduction. In the D-20Ne-HT sample, D retention falls below the TDS detection limit and cannot be quantified.

## 4. Discussion

### 4.1. The effects of Ne on surface morphology and blistering

In this study, Ne seeding markedly affects the surface morphology of W under D plasma irradiation, primarily through the formation of micro-wrinkle structures [31] caused by sputtering and the modification in blistering behavior. Under both low- and high-temperature plasma exposure, physical sputtering with varying degrees induced by Ne implantation is observed on the W surface, which is governed by the inherent properties of Ne. In all experiments conducted in this study, the incident ion energy is set to 40 eV, reaching the sputtering threshold of Ne on W.

In the low-temperature (500 K) experimental series, Ne significantly suppresses the D-induced surface blistering during the sequential Ne-D plasma exposure. However, this suppression effect is absent when Ne is seeded directly into D plasma, where blister rupture occurs instead. This discrepancy is primarily attributed to the precipitation effect of pre-existing Ne clusters on the surface. On the one hand, the presence of Ne increases the diffusion barrier of D in W, significantly impeding its migration within the W lattice [32]. Furthermore, Ne clusters localized at or near the surface preferentially combine with vacancies, forming Ne-V complexes [33]. These Ne clusters and Ne-V complexes serve as strong trapping sites for D atoms during subsequent D irradiation [34]. These effects collectively hinder D recombination and reduce blister formation. Another possible factor contributing to blister suppression is the enhanced surface roughness of W due to Ne pre-irradiation (Fig. 2 (a1)), which is unfavorable for blister formation [19,35].

Previous sequential D-Ne plasma exposure experiments conducted on Pilot-PSI [26] demonstrated that Ne pre-irradiation did not significantly suppress subsequent D-induced blistering. Micron-sized blisters were still observed on the W surface after sequential D-Ne irradiation, which contrasts with the findings of this study. The primary discrepancy is the ratio of Ne: D. Although both experiments employ a D fluence of $1.0 \times 10^{26}$ D/$m^2$, the Ne fluence in the previous study is $0.5 \times 10^{26}$ D/$m^2$ and $1.0 \times 10^{26}$ D/$m^2$. According to computational simulations by Backman et al. [36], the dynamic energetic implantation of Ne may lead to the escape of substitutional Ne atoms during subsequent high-energy Ne impacts on the W surface. Consequently, higher Ne fluence may lead to reduced Ne retention, weakening its suppression of D-induced blistering and ultimately resulting in blister formation.

A comparison of the two sets of experimental results reveals a strong correlation between the impact of Ne seed into D plasma on surface modification and temperature and ion flux. Under low-temperature conditions, the mixed D-Ne irradiated samples (mixed D-Ne-LT) lead to blister formation (Fig. 2(b1)), while blistering is completely inhibited on high-temperature irradiated samples in the Pilot-PSI setup (Fig. 4(b1) and (c1)). In our previous mixed D-Ne exposure conducted on Pilot-PSI at ~550 K [13], blistering is suppressed only under D-20Ne conditions. In contrast, D-5Ne and D-10Ne exposures still result in blister formation, although both the blister size and number density are notably reduced compared to those observed under pure D plasma irradiation. Kreter et al. [9] also indicate that compared to 500 K, D+10 %Ne irradiation at 770 K completely inhibits blistering. These observations indicate that D-Ne irradiation at elevated temperatures is more effective in suppressing D-induced blistering. Since temperature has been recognized as

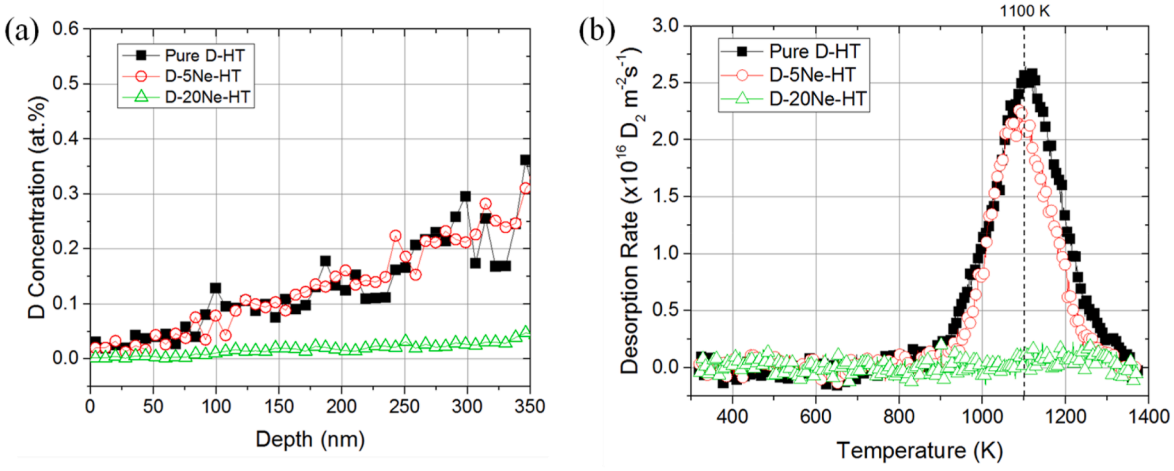


**Fig. 6.** ERDA spectra for D concentration (a) and TDS result (b) of irradiated W samples exposed to pure D and mixed D-Ne plasma at high temperature (~1200 K) conducted on Pilot-PSI.

a critical factor influencing D-induced blistering in pure D plasma irradiation. Numerous studies have shown that blistering is most severe at 500 K, while at temperatures above 500 K, hydrogen tends to escape from defects, leading to a reduction in blistering [37–39]. This temperature dependence is further supported by comparing our previous low-temperature mixed D-Ne exposure experiments on Pilot-PSI [13] with the high-temperature (~1200 K) pure D plasma exposure in this study (Fig. 4(a1) and (a3)). However, in our high-temperature series, small blisters are still observed on the surface under pure D plasma irradiation (Fig. 4(a3)), while no blistering occurred under mixed D-Ne conditions, regardless of whether the Ne fraction is D-5Ne or D-20Ne. This suggests that, in addition to the suppression effect of high temperature, Ne seeding also contributes to inhibiting blister formation. Combined with our previous low-temperature findings where blistering persisted [13], we attribute the suppression of blistering at high temperatures to the synergistic effect of temperature and Ne seeding.

To investigate the mechanism underlying the suppression of blistering by Ne seeding into D plasma at high temperatures, PADB measurements are conducted to analyze the changes of near-surface vacancy-type defect, as shown in Fig. 7. The *S-W* curve in Fig. 7 reveals the variation in the vacancy defect types in W under different plasma exposures, with the unirradiated W sample (blank W) as a reference. For mixed D-5Ne-HT, the *S-W* curve shifts upward, with a change in slope, while the mixed D-20Ne-HT has a more distinct shift. These results indicate that Ne impurity significantly changes the type and density of near-surface vacancy-type defects in W under D-Ne synergistic irradiation. Therefore, the seeding of Ne caused an upward trend in the W parameter compared to both blank W and pure D cases, and this effect intensified with increasing Ne concentration. This suggests that Ne impurity changes the vacancy-type defect structure induced by the synergistic effect of D-Ne plasma irradiation in W. Moreover, the formation of vacancy clusters generally leads to a decrease in the W parameter. Therefore, it can be inferred that, during D-Ne mixed plasma irradiation, vacancies near the surface continue to trap D atoms; however, the aggregation and growth of vacancy clusters are effectively suppressed. Ne effectively pins D-vacancy complexes to inhibit aggregation behavior. The results of PADB further validate our analysis of the suppression mechanism in low-temperature irradiation (500 K). Additionally, as the Ne concentration or dose increases, the enhancement of surface sputtering and the impact on near-surface defect characteristics become significantly more pronounced. Beyond that, as mixed D-Ne irradiation at high temperatures shows a more significant increase in surface roughness (Fig. 4(c2)), this suppression effect can be attributed to two synergistic mechanisms: First, similar to sequential D-Ne irradiation, Ne effectively inhibits D accumulation in the near-surface region by increasing the diffusion barrier and forming trapping sites. Second, the continuous physical sputtering by Ne actively removes the D-rich surface layer, enabling trapped D to be released back into the plasma or vacuum environment.

### 4.2. The impact of Ne seeding on deuterium retention

In the $D_2$ desorption spectra of W samples after irradiation, observed in Fig. 5, the desorption peak at 700 K observed on pure D-LT and mixed D-10Ne-LT can be attributed to the release of D from dislocations. Since surface blistering induces the formation of dislocations, the extent of blistering directly affects the intensity of this desorption peak. As discussed in Section 3.1, mixed D-10Ne-LT has a lower blistering density, resulting in fewer blister-induced defects and consequently a weaker desorption peak at 700 K. However, the primary desorption peak for sequential D-Ne irradiation appears at a higher temperature (~770 K), attributed to the strong trapping of D by Ne clusters. Furthermore, the additional desorption peak at ~830 K primarily results from D trapping by vacancies.

Regarding the effect of Ne on W surface damage at high temperatures, as observed in the second series of experiments conducted at the Pilot-PSI, except for the 20 % Ne implantation, the other samples display a prominent high-temperature desorption peak (~1100 K). Compared to the low-temperature irradiation [13], this high-temperature peak shifted from 820 K to 1100 K, with the 580 K low-temperature peak absent. Even at higher temperatures, when the surface concentration of D is sufficiently high, it can still be trapped by surface defects. According to Ogorodnikova et al. [40], these defects could include vacancy clusters or deuterium molecules chemically adsorbed within blisters.

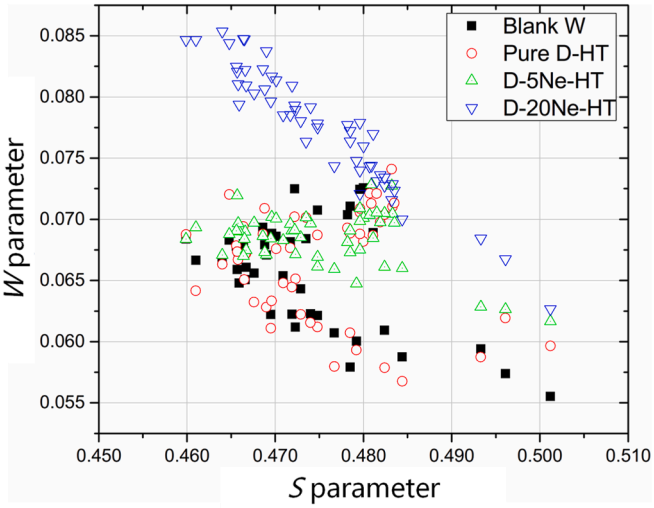


**Fig. 7.** The *S-W* values of PADB results for W samples after high-temperature pure D and mixed D-Ne plasma exposure. Note that, the PADB data of blank W is included in the spectra as a reference.

To analyze the depth distribution of D, we selected three representative test samples from the first experimental series and measured D retention within a depth of <7 μm. The results are presented in Table 1. By calculating the TDS/NRA ratio, the obtained values are 1.31 for Pure D-LT, 1.59 for sequential D-Ne, and 1.54 for mixed D-10Ne. The ratio of all three samples is > 1, indicating that the diffusion depth of D exceeds 7 μm. The minimal difference between the ratios for sequential and mixed D-Ne irradiation indicates that Ne affects the depth distribution and retention behavior of D through comparable mechanisms in both irradiation modes. Consequently, it is reasonable to conclude that the depth distribution of D is predominantly determined by D plasma conditions, particularly temperature. Furthermore, the TDS/NRA ratios for sequential and mixed D-Ne are marginally higher than those of pure D-LT. In Kreter et al.'s study [9], the TDS/NRA ratio also shows no significant difference between pure D and D-Ne mixed exposure at 500 K. However, at 770 K, Ne seeding markedly increases the ratio (>45), significantly exceeding that of pure D (~3.7). The increase in the TDS/NRA ratio due to Ne seeding may be attributed to the trapping of a significant fraction of D in near-surface regions by Ne-vacancy complexes. Simultaneously, Ne-induced sputtering removes this near-surface layer, causing the trapped D to be re-emitted into the plasma or vacuum. As a result, the reduced D concentration in the surface region leads to a higher TDS/NRA ratio in the presence of Ne seeding.

Comparing the D retention under different plasma irradiation conditions in Tables 1, it is evident that Ne significantly influences D retention in W, with effects depending on factors such as temperature and Ne implantation dose et al. Firstly, the seeding of Ne leads to a significant reduction in D retention, whether under high or low temperature conditions. At low temperatures, both Ne pre-irradiation (sequential D-Ne) and D-Ne synergy irradiation (mixed D-10Ne-LT) cause a ~50 % reduction in D retention compared to pure D irradiation at the same dose. Under high-temperature conditions, D retention in the mixed D-Ne plasma irradiation samples decreases by ~ 30 % for D-5Ne compared to pure D, while in D-20Ne samples, D retention drops to

below $10^{17}$ D/m$^2$, a value beneath the TDS detection limit and not accurately measured.

This finding is consistent with previously observed trends in D-Ne plasma irradiations at ~500 K, where, at ion energies near or below the sputtering threshold (~40 eV), Ne significantly reduces D retention [9,13,15,26,41]. This is mainly attributed to two factors. First, sputtering influences D retention through both direct and indirect mechanisms. Directly, stronger sputtering can also lead to the loss of larger surface layers of W, removing the D retention layer and allowing trapped D atoms to escape the surface, returning to the plasma or vacuum environments and reducing D retention within the bulk. The magnitude of these effects is positively correlated with Ne dose/flux, with higher doses resulting in more significant suppression of D retention. Indirectly, Ne sputtering causes surface erosion and the formation of pores at the blister caps, which increases the pathways for D diffusion outward. The second factor is the suppression of blister formation by Ne-V vacancy complexes, as blistering plays a dominant role in increasing D retention [42,43]. In sequential D-Ne irradiation, the reduction in D retention is primarily due to the suppression of D-induced blistering, thereby minimizing the contribution of D-induced blistering to overall retention.

It is worth noting that when comparing the effect of Ne on D retention between the PSI-2 and Pilot-PSI setups, the latter, with higher ion flux and influence, consistently showed lower D retention. In addition to the variations in Ne influence and temperature, the exposure time also plays a significant role. The PSI-2 experiment had a longer exposure time (~10,000 s), while the Pilot-PSI exposure time was only ~300 s. The extended exposure time in PSI-2 promotes deeper diffusion of D into the W, potentially resulting in higher D retention.

## 5. Conclusion

This study systematically investigated the influence of Ne seeding into D plasma on W surface modification and deuterium retention. Exposing W samples to pure D, sequential D-Ne, and mixed D-Ne plasmas at 500 K and 1200 K with Ne concentrations of 5 %, 10 %, and 20 % in PSI-2 and Pilot-PSI. The main findings are summarized as follows:

(1) Ne seeding alters the surface morphology and mitigates D-induced blistering. At 500 K, sequential D-Ne irradiation effectively suppresses blister formation, while mixed D-Ne irradiation results in fractured blisters due to the synergistic interaction of D and Ne. At high temperatures (~1200 K), Ne seeding entirely eliminates blistering, regardless of whether the Ne concentration is 5 % or 20 %.
(2) Deuterium retention was effectively suppressed under all applied plasma conditions. Both sequential D-Ne and mixed D-10Ne-LT exposures led to ~50 % reduction. A moderate decrease of ~30 % was observed for mixed D-5Ne-HT, whereas mixed D-20Ne-HT resulted in a reduction exceeding two orders of magnitude, with retention levels below $10^{17}$ D/m$^2$.
(3) The reduction in D retention arises from the combined effects of Ne sputtering and the Ne-vacancy complex. Ne sputtering directly removes the D-rich surface layer and indirectly induces surface erosion and pore formation at blister caps, thereby enhancing D out-diffusion pathways. Moreover, the formation of Ne-vacancy complexes suppresses blistering, further decreasing the contribution of blisters to overall D retention.

In summary, this work highlights the dual role of Ne in fusion environments: as a radiative cooling impurity to manage heat loads and as a modifier of W surface properties to suppress D retention and blistering. These findings provide a foundation for optimizing divertor materials in future fusion reactors, where controlling fuel retention and surface erosion is critical for sustained plasma performance and operational efficiency.

## CRediT authorship contribution statement

**Ying Qin:** Writing – original draft, Investigation, Formal analysis, Data curation, Conceptualization. **Long Cheng:** Writing – review & editing, Methodology, Investigation, Data curation, Conceptualization. **Yue Yuan:** Supervision, Data curation, Conceptualization. **Yuhao Li:** Writing – review & editing, Resources, Investigation. **Di Hu:** Writing – review & editing, Supervision, Methodology. **Sijie Hao:** Writing – review & editing, Supervision, Investigation. **Arkadi Kreter:** Writing – review & editing, Supervision, Resources. **Guang-Hong Lu:** Supervision, Resources, Methodology.

## Declaration of competing interest

The authors declare that they have no known competing financial interests or personal relationships that could have appeared to influence the work reported in this paper.

## Acknowledgement

This work was supported by the National Magnetic Confinement Fusion Energy R&D Program under Grant No. 2019YFE03110100, and the National Natural Science Foundation of China under Grant Nos. 12222501, 12435016 and 12275016. Dr Yue Yuan is grateful to be supported by 'the Fundamental Research Funds for the Central Universities' and the '111 center' (No. 20065). The authors would like to thank Dr. Thomas W. Morgan from DIFFER for his assistance with the Pilot-PSI experiments, Prof. Henk Schut from Delft University of Technology for his support through the PADB, and Prof. Liqun Shi from Fudan University for his support through the ERDA.

## References

[1] T. Hirai, F. Escourbiac, V. Barabash, et al., Status of technology R&D for the ITER tungsten divertor monoblock, J. Nucl. Mater. 463 (2015) 1248–1251, https://doi.org/10.1016/j.jnucmat.2014.12.027.
[2] K. Ezato, S. Suzuki, Y. Seki, et al., Progress of ITER full tungsten divertor technology qualification in Japan, Fusion Eng. Des. 98 (2015) 1281–1284, https://doi.org/10.1016/j.fusengdes.2015.03.009.
[3] A. Kallenbach, M. Bernert, R. Dux, et al., Impurity seeding for tokamak power exhaust: from present devices via ITER to DEMO, Plasma Phys. Contr. Fusion 55 (2013) 124041, https://doi.org/10.1088/0741-3335/55/12/124041.
[4] J. Schweinzer, A.C.C. Sips, G. Tardini, et al., Confinement of 'improved H-modes' in the all-tungsten ASDEX Upgrade with nitrogen seeding, Nucl. Fusion 51 (2011) 113003, https://doi.org/10.1088/0029-5515/51/11/113003.
[5] I.Y. Senichenkov, R. Ding, P.A. Molchanov, et al., SOLPS-ITER modeling of CFETR advanced divertor with Ar and Ne seeding, Nucl. Fusion 62 (2022) 096010, https://doi.org/10.1088/1741-4326/ac75da.
[6] V. Philipps, Tungsten as material for plasma-facing components in fusion devices, J. Nucl. Mater. 415 (2011) S2–S9, https://doi.org/10.1016/j.jnucmat.2011.01.110.
[7] H. Zhang, H.W. Zhang, L. Qiao, et al., Erosion and deuterium retention behavior of tungsten exposed to impurity-seeded deuterium plasma, Tungsten 3 (2021) 448–458, https://doi.org/10.1007/s42864-021-00106-5.
[8] A. Kallenbach, M. Balden, R. Dux, et al., Plasma surface interactions in impurity seeded plasmas, J. Nucl. Mater. 415 (2011) S19–S26, https://doi.org/10.1016/j.jnucmat.2010.11.105.
[9] A. Kreter, D. Nishijima, R.P. Doerner, et al., Influence of plasma impurities on the fuel retention in tungsten, Nucl. Fusion 59 (2019) 086029, https://doi.org/10.1088/1741-4326/ab235d.
[10] O.V. Ogorodnikova, K. Sugiyama, A. Markin, et al., Effect of nitrogen seeding into deuterium plasma on deuterium retention in tungsten, Phys. Scri. (T145) (2011) 014034, https://doi.org/10.1088/0031-8949/2011/T145/014034.
[11] L. Gao, W. Jacob, G. Meisl, et al., Interaction of deuterium plasma with sputter-deposited tungsten nitride films, Nucl. Fusion 56 (2015) 016004, https://doi.org/10.1088/0029-5515/56/1/016004.
[12] M. Ishida, H.T. Lee, Y. Ueda, The influence of neon or argon impurities on deuterium permeation in tungsten, J. Nucl. Mater. 463 (2015) 1062–1065, https://doi.org/10.1016/j.jnucmat.2014.11.123.
[13] L. Cheng, G. De Temmerman, T.W. Morgan, et al., Mitigated blistering and deuterium retention in tungsten exposed to high-flux deuterium–neon mixed plasmas, Nucl. Fusion 57 (2017) 046028, https://doi.org/10.1088/1741-4326/aa5c5c.
[14] M. Backman, K.D. Hammond, F. Sefta, et al., Atomistic simulations of tungsten surface evolution under low-energy neon implantation, Nucl. Fusion 56 (2016) 046008, https://doi.org/10.1088/0029-5515/56/4/046008.

[15] Y. Yuan, T. Wang, A. Kreter, et al., Influence of neon seeding on the deuterium retention and surface modification of ITER-like forged tungsten, Nucl. Fusion 61 (2021) 016007, https://doi.org/10.1088/1741-4326/abbc86.
[16] M. Rasinski, A. Kreter, Y. Torikai, et al., The microstructure of tungsten exposed to D plasma with different impurities, Nucl. Mater. Energy 12 (2017) 302–306, https://doi.org/10.1016/j.nme.2016.11.001.
[17] R.A. Pitts, S. Carpentier, F. Escourbiac, et al., A full tungsten divertor for ITER: physics issues and design status, J. Nucl. Mater. 438 (2013) S48–S56, https://doi.org/10.1016/j.jnucmat.2013.01.008.
[18] Y. Yuan, H. Greuner, B. Böswirth, et al., Recrystallization and grain growth behavior of rolled tungsten under VDE-like short pulse high heat flux loads, J. Nucl. Mater. 433 (2013) 523–530, https://doi.org/10.1016/j.jnucmat.2012.04.022.
[19] M.C. Ren, Y. Yuan, F. Feng, et al., Deuterium retention in cyclic transient heat loaded tungsten with increasing cycle numbers, Nucl. Fusion 64 (2024) 056021, https://doi.org/10.1088/1741-4326/ad36d5.
[20] Y. Yuan, H. Greuner, B. Böswirth, et al., Recrystallization and grain growth behavior of rolled tungsten under VDE-like short pulse high heat flux loads, J. Nucl. Mater. 433 (1–3) (2013) 523–530, https://doi.org/10.1016/j.jnucmat.2012.04.022.
[21] M. Reinhart, A. Pospieszczyk, B. Unterberg, et al., Using the radiation of hydrogen atoms and molecules to determine electron density and temperature in the linear plasma device PSI-2, Fusion Sci. Technol. 63 (2013) 201–204, https://doi.org/10.13182/FST13-A16905.
[22] A. Kreter, C. Brandt, A. Huber, et al., Linear plasma device PSI-2 for plasma-material interaction studies, Fusion Sci. Technol. 68 (2015) 8–14, https://doi.org/10.13182/FST14-906.
[23] M. Miyamoto, D. Nishijima, Y. Ueda, et al., Observations of suppressed retention and blistering for tungsten exposed to deuterium–helium mixture plasmas, Nucl. Fusion 49 (2009) 065035, https://doi.org/10.1088/0029-5515/49/6/065035.
[24] P. Fiflis, N. Connolly, D.N. Ruzic, Experimental mechanistic investigation of the nanostructuring of tungsten with low energy helium plasmas, J. Nucl. Mater. 482 (2016) 201–209, https://doi.org/10.1016/j.jnucmat.2016.10.015.
[25] H. Maecker, Ein zylindrischer Bogen für hohe Leistungen, Z. Naturforsch. 11 (6) (1956) 457–459, https://doi.org/10.1515/zna-1956-0606.
[26] L. Cheng, G. De Temmerman, P.A.Z. Van Emmichoven, et al., Effect of neon plasma pre-irradiation on surface morphology and deuterium retention of tungsten, J. Nucl. Mater. 463 (2015) 1025–1028, https://doi.org/10.1016/j.jnucmat.2014.11.110.
[27] A. Vehanen, K. Saarinen, P. Hautojärvi, et al., Profiling multilayer structures with monoenergetic positrons, Phys. Rev. B 35 (1987) 4606, https://doi.org/10.1103/PhysRevB.35.4606.
[28] H.Y. Xu, G.N. Luo, H. Schut, et al., Enhanced modification of tungsten surface by nanostructure formation during high flux deuterium plasma exposure, J. Nucl. Mater. 447 (2014) 22–27, https://doi.org/10.1016/j.jnucmat.2013.12.010.
[29] B. Tyburska-Püschel, K. Ertl, M. Mayer, et al., Saturation of deuterium retention in self-damaged tungsten exposed to high-flux plasmas, Nucl. Fusion 52 (2012) 023008, https://doi.org/10.1088/0029-5515/52/2/023008.
[30] Y.Z. Jia, W. Liu, B. Xu, et al., Nanostructures and pinholes on W surfaces exposed to high flux D plasma at high temperatures, J. Nucl. Mater. 463 (2015) 312–315, https://doi.org/10.1016/j.jnucmat.2014.11.054.
[31] S. Takamura, Y. Uesugi, A.M. Ito, et al., Microwrinkle structures on refractory metal surfaces irradiated with noble gas plasma species, Nucl. Fusion 57 (2017) 086043, https://doi.org/10.1088/1741-4326/aa75ee.
[32] X.S. Kong, J. Hou, X.Y. Li, et al., First principles study of inert-gas (helium, neon, and argon) interactions with hydrogen in tungsten, J. Nucl. Mater. 487 (2017) 128–134, https://doi.org/10.1016/j.jnucmat.2017.01.038.
[33] Y.H. Li, H.B. Zhou, G.H. Lu, Towards understanding the strong trapping effects of noble gas elements on hydrogen in tungsten, Int. J. Hydrogen Energy 42 (2017) 6902–6917, https://doi.org/10.1016/j.ijhydene.2016.12.151.
[34] Y.L. Liu, Y. Zhang, H.B. Zhou, et al., Vacancy trapping mechanism for hydrogen bubble formation in metal, Phys. Rev. B Condens. Matter 79 (2009) 172103, https://doi.org/10.1103/PhysRevB.79.172103.
[35] A. Manhard, M. Balden, U. Von Toussaint, Blister formation on rough and technical tungsten surfaces exposed to deuterium plasma, Nucl. Fusion 57 (12) (2017) 126012, https://doi.org/10.1088/1741-4326/aa82c8.
[36] M. Backman, K.D. Hammond, F. Sefta, et al., Atomistic simulations of tungsten surface evolution under low-energy neon implantation, Nucl. Fusion 56 (4) (2016) 046008, https://doi.org/10.1088/0029-5515/56/4/046008.
[37] V.K. Alimov, W.M. Shu, J. Roth, et al., Temperature dependence of surface topography and deuterium retention in tungsten exposed to low-energy, high-flux D plasma, J. Nucl. Mater. 417 (1–3) (2011) 572–575, https://doi.org/10.1016/j.jnucmat.2011.01.088.
[38] V.K. Alimov, B. Tyburska-Püschel, S. Lindig, et al., Temperature dependence of surface morphology and deuterium retention in polycrystalline ITER-grade tungsten exposed to low-energy, high-flux D plasma, J. Nucl. Mater. 420 (1–3) (2012) 519–524, https://doi.org/10.1016/j.jnucmat.2011.11.003.
[39] W.M. Shu, K. Isobe, T. Yamanishi, Temperature dependence of blistering and deuterium retention in tungsten exposed to high-flux and low-energy deuterium plasma, Fusion Eng. Des. 83 (7–9) (2008) 1044–1048, https://doi.org/10.1016/j.fusengdes.2008.05.006.
[40] O.V. Ogorodnikova, J. Roth, M. Mayer, Deuterium retention in tungsten in dependence of the surface conditions, J. Nucl. Mater. 313 (2003) 469–477, https://doi.org/10.1016/S0022-3115(02)01375-2.
[41] T.J. Finlay, J.W. Davis, T. Schwarz-Selinger, et al., Deuterium retention in recrystallized tungsten irradiated with simultaneous deuterium–neon ion beams, Nucl. Mater. Energy 12 (2017) 1288–1293, https://doi.org/10.1016/j.nme.2016.12.027.
[42] M. Liu, W. Guo, L. Cheng, et al., Blister-dominated retention mechanism in tungsten exposed to high-fluence deuterium plasma, Nucl. Fusion 60 (12) (2020) 126034, https://doi.org/10.1088/1741-4326/abb600.
[43] C. Li, L. He, H. Tu, et al., Deuterium trapping behavior in tungsten surface due to low-energy ion irradiation, J. Nucl. Mater. 577 (2023) 154336, https://doi.org/10.1016/j.jnucmat.2023.154336.